Development 138, 339-348 (2011) doi:10.1242/dev.054056

Ripply3, a Tbx1 repressor, is required for development of the pharyngeal apparatus and its derivatives in mice

Tadashi Okubo[1,2], Akinori Kawamura[1,*], Jun Takahashi[1,2], Hisato Yagi[3], Masae Morishima[3,4], Rumiko Matsuoka[3,4] and Shinji Takada[1,2,†]

SUMMARY

The pharyngeal apparatus is a transient structure that gives rise to the thymus and the parathyroid glands and also contributes to the development of arteries and the cardiac outflow tract. A typical developmental disorder of the pharyngeal apparatus is the 22q11 deletion syndrome (22q11DS), for which *Tbx1* is responsible. Here, we show that Ripply3 can modulate Tbx1 activity and plays a role in the development of the pharyngeal apparatus. *Ripply3* expression is observed in the pharyngeal ectoderm and endoderm and overlaps with strong expression of *Tbx1* in the caudal pharyngeal endoderm. Ripply3 suppresses transcriptional activation by Tbx1 in luciferase assays in vitro. *Ripply3*-deficient mice exhibit abnormal development of pharyngeal derivatives, including ectopic formation of the thymus and the parathyroid gland, as well as cardiovascular malformation. Corresponding with these defects, *Ripply3*-deficient embryos show hypotrophy of the caudal pharyngeal apparatus. Ripply3 represses Tbx1-induced expression of *Pax9* in luciferase assays in vitro, and *Ripply3*-deficient embryos exhibit upregulated *Pax9* expression. Together, our results show that Ripply3 plays a role in pharyngeal development, probably by regulating Tbx1 activity.

KEY WORDS: Ripply3, Tbx1, Cardiovascular, Endoderm, Pharyngeal arch, Thymus, Mouse

INTRODUCTION

The pharyngeal apparatus is a transient structure that is formed ventrolateral to the hindbrain in vertebrate embryos. It consists of bilaterally segmented arches, between which ectodermal grooves and endodermal pouches are formed. The pharyngeal arches comprise mesodermal cells, neural crest-derived mesenchyme, an outer ectodermal cover, and an inner endodermal lining. Within the arches, pharyngeal arch arteries (PAAs) also develop. Components of the pharyngeal apparatus give rise to distinct tissues at later stages of development. For instance, the pharyngeal arteries and neural crest cells in the caudal pharyngeal arches contribute to cardiovascular development, whereas the endodermal cells located in the caudal pouches give rise to several organs, including the thymus and parathyroid gland. Thus, pharyngeal development is a key process in the generation of these organs.

Chromosome 22q11 deletion syndrome (22q11DS), which includes the DiGeorge syndrome (DGS), conotruncal anomaly face syndrome (CAFS) and velocardiofacial syndrome (VCFS), is characterized by the abnormal development of the pharyngeal apparatus in the form of thymic hypoplasia or aplasia, hypocalcemia arising from parathyroid hypoplasia, and defective cardiac outflow (Scambler, 2000). A number of mouse genetic studies and mutation analyses in human patients have indicated that *Tbx1*, which encodes a member of the T-box family of transcription factors, is most likely responsible for the phenotype of 22q11DS (Jerome and Papaioannou, 2001; Lindsay et al., 2001; Merscher et al., 2001; Yagi et al., 2003). During murine pharyngeal development, *Tbx1* is first expressed in the mesoderm at E7.5. Between E8.5 and E11.5, *Tbx1* expression appears in the pharyngeal endoderm, ectoderm and core mesoderm, but not in the neural crest cells (Chapman et al., 1996; Vitelli et al., 2002; Yamagishi et al., 2003). Cell type-specific inactivation and analysis of downstream targets of *Tbx1* in mice indicate that *Tbx1* plays multiple roles in endoderm, mesoderm and ectoderm cells during pharyngeal development (Arnold et al., 2006; Zhang et al., 2006; Calmont et al., 2009). However, the molecular mechanisms underlying the cell type-specific roles of Tbx1 have not been fully elucidated.

T-box transcription factors are characterized by their DNA-binding domain, known as the T-domain, and function as either activators or repressors depending on their association with transcriptional co-activator or co-repressor complexes. Tbx1 is known to act as a transcriptional activator as it activates the transcription of a reporter containing the T-box binding elements in vitro and in vivo (Xu et al., 2004; Hu et al., 2004; Stoller and Epstein, 2005; Paylor et al., 2006; Zweier et al., 2007). However, in addition to the 'on DNA' manner, Tbx1 also functions in an 'off DNA' manner by interfering with Smad1-Smad4 binding in the regulation of BMP signaling (Fulcoli et al., 2009). Despite an accumulation of studies on transgenic and mutant mouse lines, the molecular basis underlying Tbx1-mediated gene regulation in pharyngeal development remains to be elucidated.

Ripply proteins have recently been shown to modulate the transcriptional properties of T-box proteins (Kawamura et al., 2008; Kondow et al., 2007). Ripply associates with the transcriptional co-repressor Groucho/TLE and the T-box proteins through two distinct amino acid sequences: the WRPW motif, which is a highly

[1]Okazaki Institute for Integrative Bioscience, National Institutes of Natural Sciences, Okazaki, Aichi 444-8787, Japan. [2]Department of Basic Biology, Graduate University for Advanced Studies (SOKENDAI), Okazaki, Aichi 444-8787, Japan. [3]International Research and Educational Institute for Integrated Medical Sciences, Tokyo Women's Medical University, Shinjuku-ku, Tokyo 162-8666, Japan. [4]Department of Pediatric Cardiology, Tokyo Woman's Medical University, Shinjuku-ku, Tokyo 162-8666, Japan.

*Present address: Department of Life Science, Graduate School of Science and Engineering, Saitama University, Sakura-ku, Saitama 338-8570, Japan
†Author for correspondence (stakada@nibb.ac.jp)

Accepted 1 November 2010

conserved four amino acid stretch in the N-terminal half; and the Ripply homology (RH) domain, a conserved ~50 amino acid stretch that interacts with the T-domain (Kawamura et al., 2005; Kondow et al., 2006). Therefore, Ripply is able to recruit the Groucho/TLE co-repressor to T-box proteins and control their intrinsic transcriptional properties. *Ripply1* and *Ripply2* have been shown to play roles in somite segmentation during development (Kawamura et al., 2005; Kondow et al., 2007; Morimoto et al., 2007; Chan et al., 2007; Moreno et al., 2008; Takahashi et al., 2010).

To reveal the developmental role of another member of the Ripply family, *Ripply3* [also known as Down syndrome critical region 6 (*Dscr6*)] (Kawamura et al., 2005; Hitachi et al., 2009; Shibuya et al., 2000), we examined its expression and function in the early mouse embryo. On finding that both *Ripply3* and *Tbx1* are expressed in the pharyngeal endoderm, we examined the role of Ripply3 by generating *Ripply3*-deficient mice and investigated its relationship with Tbx1.

MATERIALS AND METHODS

In situ hybridization and immunohistochemical staining

Whole-mount in situ hybridization was performed as described previously (Yoshikawa et al., 1997). In situ hybridization was also carried out on 7-μm paraffin sections collected from embryos. Paraffin sections (7 μm) were also incubated with antibodies specific for Tbx1 (ab18530, Abcam), Pax9 (clone 7C2, Sigma), AP-2α (3B5, DSHB), phospho-histone H3 (Ser10, Millipore Upstate), Nkx2.1 (TTF1; clone 8G7G3/1, Dako) and Pecam1 (CD31; clone MEC13.3, BD Pharmingen). The secondary antibodies and signal amplification used were anti-rat IgG-Alexa Fluor 488, anti-rabbit IgG-Alexa Fluor 546 (Molecular Probes) and the EnVision System-HRP (Dako). For the TUNEL assay, the In Vitro Cell Death Detection Kit-TM-Red was used (Roche).

Gene targeting

For the generation of *Ripply3*-deficient mice, a mouse *Ripply3* genomic clone was obtained from 129SV genomic DNA by PCR. An *IRES-lacZ-PGK-neo* cassette, in which the neomycin phosphotransferase gene is linked to the *lacZ* gene placed between the independent ribosomal entry sequence (IRES) and an SV40 polyadenylation signal (Ohbayashi et al., 2002), replaced a sequence covering the *Ripply3* coding sequence of the first, second and third exons. The diphtheria toxin A (DTA) expression cassette was inserted at the 3′ end of the genomic DNA.

Embryonic stem (ES) cells and mouse strains

CJ7 ES cells were electroporated with linearized targeting vector and selected in media containing G418. Targeted clones were confirmed by PCR and Southern blot analysis. Heterozygous ES cells were injected into blastocysts of C57BL/6J mice to generate germline chimeras. Chimeric males were mated with C57BL/6J females, and heterozygous mice were subsequently backcrossed onto either C57BL/6J or 129SV strains. No obvious phenotypic differences were observed between the mice generated on the C57BL/6J or 129SV backgrounds. *Tbx1* knockout mice were kindly provided by Dr Bernice Morrow [Albert Einstein College, NY, USA (Merscher et al., 2001)] and maintained as heterozygous lines.

Genotyping

For genotyping, the wild-type or mutant alleles were amplified by PCR using the following primers (5′ to 3′): Rpy3-geF1, AACCTGAGATC-GACTACTGC; Rpy3-geR1, ATCCCTTAAGGTCTGTCTGC; lacZ-F1, TGTTTTGACCGCTGGGATCTGC; and lacZ-R1, CCAGACCAACTG-GTAATGGTAGC. Amplification was performed for 32 cycles at 94°C for 30 seconds, 60°C for 30 seconds, and 72°C for 30 seconds. The presence of a 350 bp fragment, a 550 bp fragment or both fragments represented animals of wild-type, *Ripply3* homozygous and *Ripply3* heterozygous genotypes, respectively. PCR genotyping of *Tbx1* alleles was as previously described (Merscher et al., 2001).

RT-PCR

Total RNA was extracted from tissues or whole embryos using RNeasy (Qiagen). cDNA was synthesized using SuperScript III reverse transcriptase (Invitrogen) with oligo(dT) primers. Primer sequences (5′ to 3′) were as follows: beta-actin (*Actb*), TCGTACCACAGGCATTGTGATGG and GCAATGCCTGGGTACATGGTGG; *Ripply3*, F2 GTCGGTCTGAGA-GATTCGCG and R4 CTTTATTCTGCCCTTTCCTCC.

Luciferase assay

For luciferase assays, COS-7 cells were cultured at 37°C in Dulbecco's Modified Eagle's Medium (DMEM) supplemented with 10% fetal bovine serum (FBS). Then, 5000 cells/well were seeded into 24-well plates (Iwaki). Following overnight incubation, the cells were transiently transfected with plasmid DNA, which included pcDNA3.1-mTbx1, pcDNA3.1-mRipply3, and a T-box reporter vector that has two T-box motifs (cgcgtAAATTCACACCTgggcccAAATTCACACCTc) inserted into the *Mlu*I and *Xho*I sites of the pGL3-Promoter vector (Promega). The total DNA concentration was made consistent in each transfection by supplementation with pcDNA3.1 empty vector. A 3.7 kb stretch of the 5′ upstream region of the mouse *Pax9* gene was amplified from C57BL/6 genomic DNA using *Mlu*I or *Xho*I site-attached primers (5′-cgacgcgtcgGAAAACTTCCCCCAGACAGCTGC-3′, 5′-ccgctcgagcgg-TGCTCTGAGCAGTACACCAACC-3′). The PCR fragment was cloned into the pGL3-Basic vector (Promega) and the sequence checked. For measurement of luciferase activity, cells were harvested 24 hours after transfection and suspended in Dual-Luciferase Assay Solution (from the Dual-Glo Luciferase Assay System, Promega). For normalization of transfection efficiency, the cells were co-transfected with pRL-CMV carrying *Renilla* luciferase under the control of the CMV promoter. All experiments were undertaken in triplicate and statistical significance was evaluated.

Immunoprecipitation assay

COS-7 cells were transfected with pCS2-mRipply3-Flag, pcDNA3.1-mTbx1-myc or pcDNA3.1-mTbx1(ΔTbox)-myc using the FuGENE 6 transfection reagent (Roche). Cell lysates were incubated with anti-Flag M2-conjugated agarose gel (Sigma) or anti-Myc (4A6) agarose conjugate (Millipore) at 4°C overnight, and immunoblotting was performed with anti-myc (clone 4A6, Upstate) and anti-Flag D8 (Santa Cruz) antibodies and HRP-labeled anti-rabbit IgG (Jackson ImmunoResearch).

Flow cytometry

Antibodies used for flow cytometry included FITC-conjugated anti-mouse CD4 (L3T4; eBioscience) and PE-conjugated anti-mouse CD8a (Ly-2; eBioscience). For flow cytometry, thymocytes were isolated from the newborn thymus and the total cell number was calculated. A total of 1×10^6 cells were then incubated with a combination of the CD4 and CD8 antibodies for 30 minutes on ice, and the cells were washed three times in PBS containing bovine serum albumin before the final addition of PE for the elimination of dead cells. Flow analysis was undertaken using an Epics ALTRA flow cytometer (Beckman Coulter).

RESULTS

Ripply3 expression in the mouse embryo

To examine the spatiotemporal expression of *Ripply3* during embryogenesis, we first performed in situ hybridization and found it to be dynamically expressed in the pharyngeal endoderm and ectoderm (Fig. 1A-E). In the mouse embryo, pharyngeal arches develop in a rostral-to-caudal manner. At E8.5, when the first arch formation is observed, *Ripply3* signals were observed in the pharyngeal ectoderm (Fig. 1A,A′). After E8.5, in accordance with subsequent formation of more caudal pharyngeal arches, *Ripply3* expression was evident in the ectoderm and endoderm cells of most of the pharyngeal pouches, although its expression in the anterior pouches had started to gradually decrease. By E10.5, strong *Ripply3* expression only remained in the fourth pouch. *Ripply3* and *Tbx1* were strongly co-expressed in the endoderm around a newly

forming pouch, although *Ripply3* expression was more sustained in the anterior pouch, and *Tbx1* expression was also identified in the mesodermal cores of the pharyngeal arches (Fig. 2A). These results suggest that Ripply3 might regulate Tbx1 function specifically in the developing caudal pharyngeal endoderm, but not in the mesodermal cells, of the arches.

Ripply3-mediated repression of Tbx1 transcriptional activity

It has been proposed that Ripply proteins repress the transcriptional activities of some T-box proteins by recruiting the Groucho/TLE-HDAC complex. To examine whether mouse Ripply3 was able to repress Tbx1 transcriptional activity, we performed luciferase reporter assays in COS-7 cells, in which the reporter gene was under the control of tandemly repeated T-box protein binding sites (Fig. 2B). We found that Tbx1 significantly activated the luciferase activity in a manner that was dependent on the T-domain, whereas Ripply3 inhibited it (Fig. 2B). Immunoprecipitation assays showed that Ripply3 physically interacted with Tbx1 in a T-domain-dependent manner (Fig. 2C). As zebrafish Ripply1 is known to interact with the transcriptional co-repressor Groucho/TLE via the WRPW motif of the former (Kawamura et al., 2005), the effect of removing the WRPW motif was also examined. Compared with the wild-type Ripply3 protein, Ripply3 lacking the WRPW tetrapeptide failed to efficiently repress Tbx1-mediated enhancement of luciferase activity (Fig. 2B). Thus, Ripply3 is able to repress the transcriptional activity of Tbx1, probably by recruiting the Groucho/TLE-HDAC complex via its WRPW motif.

Next, we asked whether Ripply3 could also repress the in vitro expression of a Tbx1 target gene that is known to be expressed in the pharyngeal endoderm. Microarray analyses have suggested a number of putative downstream genes of Tbx1 in the pharyngeal endoderm (Ivins et al., 2005; Liao et al., 2008). We found that the expression of a putative endodermal target, *Pax9*, substantially overlapped that of Tbx1 (Fig. 2D). Furthermore, expression from the *Pax9* promoter was actually activated by Tbx1 in luciferase reporter assays (Fig. 2E) and Ripply3 repressed this Tbx1-mediated expression of Pax9. However, we found that even a 0.5 kb promoter fragment of *Pax9*, which does not contain a typical T-box binding site (see Fig. S1 in the supplementary material), was also regulated by Tbx1 and Ripply3. Therefore, in the case of *Pax9* expression, Tbx1 and Ripply3 might regulate this expression in an atypical manner; for instance, through some DNA element that differs from the consensus sequence of the T-box binding site or through an 'off DNA' interaction with some other component of the transcriptional machinery.

Generation of the *Ripply3* knockout mouse

To reveal the roles of *Ripply3* during embryogenesis, we generated a mutant allele of mouse *Ripply3* by inserting the *IRES-lacZ-polyA* cassette and *PGK-neo* gene into its first exon (Fig. 3A-C). As most of the amino acid sequence of Ripply3 is deleted in the protein encoded by this allele, the resulting targeted allele was expected to be null. Mice heterozygous for this mutation were found to be viable, fertile and morphologically normal (Fig. 3D). Mice homozygous for this mutation were born, but died with cyanosis within 24 hours of birth (Fig. 3D; see Table S1 in the supplementary material).

Abnormal cardiovascular development in *Ripply3*-deficient mouse embryos

This lethality with cyanosis prompted us to investigate cardiovascular development in the *Ripply3*-deficient embryos. The PAAs that pass through the pharyngeal arches to connect the aortic sac with the dorsal aorta are remodeled during development to form the mature aortic arch and great vessels (Srivastava and Olson, 2000). In wild-type embryos, the PAAs initially form as many pairs of symmetrical vessels. The first and second pairs of PAAs, as well as the right sixth PAA, regress during development. By contrast, the left fourth PAA contributes to the formation of the aortic arch, the third pair and the right fourth PAAs develop into the common carotid arteries and the right subclavian artery, respectively, and the left sixth PAA gives rise to a part of the pulmonary arteries and ductus arteriosus. Intracardiac ink injection and immunostaining with anti-Pecam1 (Baldwin et al., 1994) indicated that, in the *Ripply3*$^{-/-}$ embryos, the third and fourth PAAs could not be identified (Fig. 4A-D; see Fig. S2 in the supplementary material). By contrast, the second PAAs, which normally disappear during mammalian development, persisted and remained connected to the dorsal aorta.

These abnormalities appear to have resulted in misshapen great vessels (Fig. 4E-J). The persisting second PAAs contributed abnormally to the development of the common carotid arteries (Fig. 4G,J, asterisks). Dorsolateral to these common carotid arteries, two additional ascending arteries were ectopically formed. These arteries are likely to have been generated from the dorsal aorta, a part of which regresses in normal development (Fig. 4H,J, #). Owing to the lack of the fourth PAAs, interruption of the aortic arch occurred. Subclavian arteries in *Ripply3*$^{-/-}$ mutants were present, but they abnormally branched from the dorsal aorta in the retroesophageal region (Fig. 4H,J). The ductus arteriosus in *Ripply3*$^{-/-}$ mutants persisted and anastomosed with the descending dorsal aorta (Fig. 4G,H,J). All of these structural defects appeared to have been caused by the inappropriate persistence and regression of PAAs in the mutants. In addition to aortic arch malformation, the ventricular septum was incompletely formed in the heart of *Ripply3*$^{-/-}$ embryos. *Ripply3*$^{-/-}$ embryos also exhibited a hypotrophic aorta in the conotruncus region, in spite of the formation of outflow septum (Fig. 4K,L; see Fig. S3 in the supplementary material). Based on these findings, we concluded that Ripply3 deficiency leads to severe defects in the development of the great arteries and heart.

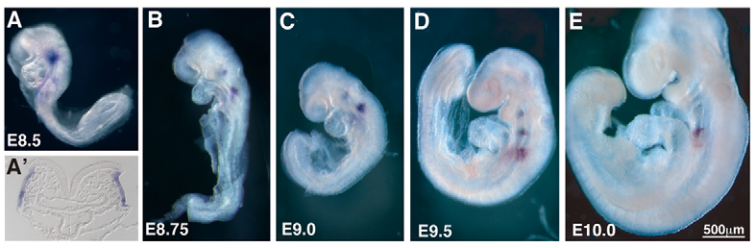

Fig. 1. Expression pattern of *Ripply3* during mouse pharyngeal arch development. (**A-E**) Whole-mount in situ hybridization for mouse *Ripply3* at E8.5 (A,A'), E8.75 (B), E9.0 (C), E9.5 (D) and E10.0 (E). A transverse section of an E8.5 embryo hybridized with the *Ripply3* probe indicates that *Ripply3* is expressed in the ectoderm at this stage (A'). Scale bar: 500 μm.

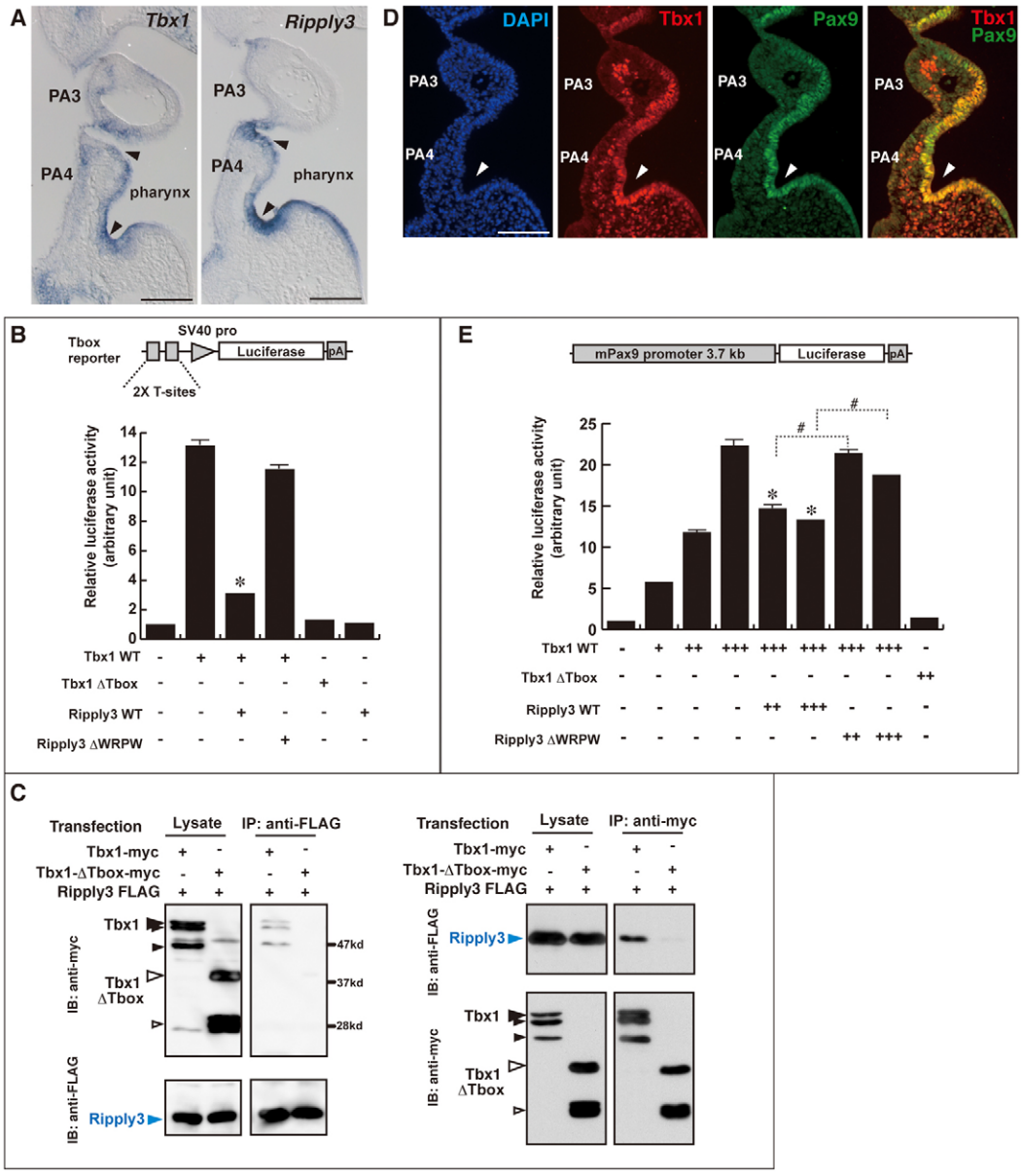

Fig. 2. Repression of the transcriptional activity of Tbx1 by Ripply3. (**A**) Expression of *Tbx1* and *Ripply3* in paracoronal sections of the pharynx region at E9.75. Arrowheads indicate pharyngeal pouches. (**B**) Repression of Tbx1 activity by Ripply3. The structure of the T-box reporter gene is shown at the top. Luciferase reporter assays show that wild-type (WT) Ripply3 antagonizes *Tbx1*-dependent transcriptional activity, whereas a deletion form of Ripply3 that lacks the WRPW motif (ΔWRPW) does not suppress this activity efficiently. (**C**) Immunoprecipitation assays for Tbx1 and Ripply3. As a control, a deletion form of Tbx1 that lacks the T-domain (Tbx1-ΔTbox) was also used. Tbx1 and Ripply3 proteins were fused with Myc and Flag tags, respectively. Tbx1 and Tbx1-ΔTbox were detected in multiple bands, some of which might arise from protein degradation. Black and white arrowheads indicate positions of Tbx1 and Tbx1-ΔTbox bands. Large arrowheads indicate the positions of predicted full-length products from each construct. (**D**) Immunofluorescence staining for Tbx1 and Pax9 in pharyngeal arches at E9.5. Nuclear staining with DAPI and a merged image of Tbx1 and Pax9 immunostaining are also shown. Arrowheads indicate pharyngeal pouches. (**E**) Repression of Tbx1-mediated *Pax9* expression by Ripply3. The structure of the mouse *Pax9* reporter gene is shown at the top. Luciferase reporter assays showed that expression from the 3.7 kb promoter of *Pax9* is activated by Tbx1 and that this activation is repressed by Ripply3 in a dose-responsive manner. * and #, $P<0.001$ by one-way ANOVA. Error bars indicate mean + s.e.m. PA, pharyngeal arch. Scale bars: 100 μm.

Abnormal development of organs derived from pharyngeal pouches in *Ripply3*-deficient embryos

In addition to the cardiovascular defects in *Ripply3*$^{-/-}$ embryos, we also found defects in the development of the thymus, the parathyroid glands and the ultimobranchial bodies, all of which are derived from the pharyngeal pouch endoderm. The endodermal cells around the third pharyngeal pouches give rise to the thymus and parathyroid glands, and those of the fourth pouch give rise to the ultimobranchial bodies (Manley and Capecchi, 1998). These organs bud from the pharyngeal pouches and migrate ventrocaudally to their final position in the mature mouse. The thymus moves to a position just anterior to the heart (Fig. 5A),

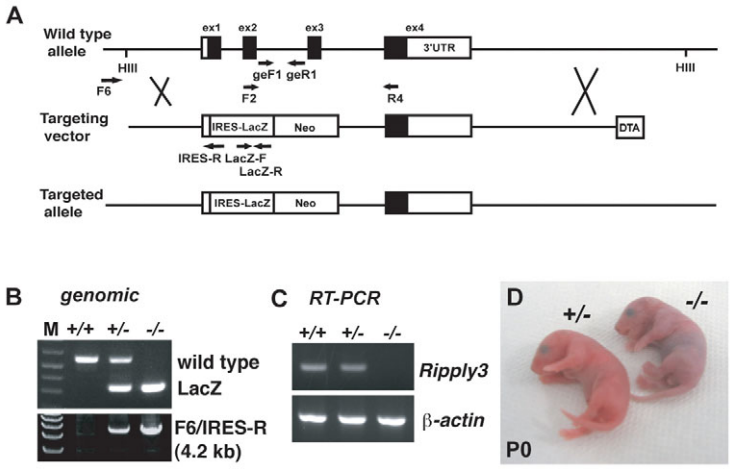

Fig. 3. Generation of the *Ripply3* knockout mouse. (**A**) Knockout strategy for the *Ripply3* locus. The *IRES-lacZ-PGK-neo* cassette replaced exons 1-3. Primers (see Materials and methods) are indicated by arrows. DTA, diphtheria toxin A expression cassette. HIII, *Hin*dIII. (**B**) *Ripply3* genotyping results obtained by genomic PCR. (**C**) RT-PCR for *Ripply3* and β-actin (*Actb*) mRNAs in E9.5 embryos. (**D**) Postnatal lethality with cyanosis in a *Ripply3*$^{-/-}$ pup at P0.

whereas the parathyroid glands and the ultimobranchial bodies move to their distinct positions either adjacent to, or within, the thyroid gland.

In the *Ripply3*$^{-/-}$ embryos, these organs were not separated from the endodermal epithelia in the pharyngeal region. For instance, the thymus, defined by *Foxn1* expression (Gordon et al., 2001), was formed but not separated from the pharyngeal endoderm at E13.5 (Fig. 5A,B,H,I). As a result, the thymus did not migrate caudally but developed ectopically in the pharynx region at E18.5 (see Fig. S4 in the supplementary material). In many cases, the ectopic thymus appeared to have evaginated into the oropharynx (Fig. 5B,D). Although the ectopic thymus was smaller than normal (Fig. 5E,F), the differentiation of thymocytes, as assessed by CD4 and CD8 expression, appeared to be normal at birth (Fig. 5G). Similarly, the primordia of the parathyroid glands, as defined by *Gcm2* expression (Gordon et al., 2001), remained attached to the endodermal epithelium and were smaller than normal (Fig. 5J,K). In addition, the primordia of the ultimobranchial bodies, which were characterized by their modest expression of *Nkx2.1* (Kusakabe et al., 2006), also failed to separate from the epithelium in the pharyngeal pouch (Fig. 5L,M). By contrast, no obvious abnormalities were identified in the derivatives of the first and second pharyngeal pouches, including the thyroid gland, which was defined on the basis of its strong *Nkx2.1* expression (Fig. 5L,M). Thus, *Ripply3* appears to be required for the development and separation of organs derived from the pharyngeal pouches.

Abnormal development of the pharyngeal apparatus in *Ripply3*-deficient mouse embryos

The defects described above suggested that the development of the pharyngeal apparatus was defective in the *Ripply3*$^{-/-}$ embryos. Therefore, we examined the morphology of the pharyngeal apparatus of the *Ripply3*$^{-/-}$ embryos at E9.5 and E10.5. Although the formation of the first and second arches was normal in the *Ripply3*$^{-/-}$ embryos, the third and fourth arches were severely reduced in size, and the ectoderm and endoderm layers were almost adjacent to each other in this region (Fig. 6A-F). In this caudal pharyngeal region, apoptotic cell death had increased dramatically (Fig. 6G,H), whereas the rate of cell proliferation had not obviously changed (Fig. 6I,J). Thus, the reduction in the size of the third and fourth arches in *Ripply3*$^{-/-}$ embryos appeared to have been due to increased cell death. Because *Ripply3* was expressed in the pharyngeal endoderm and adjacent ectoderm, but not in the mesoderm, of the pharyngeal arches, the defect in cell survival within the pharyngeal arches was likely to be a secondary consequence of defective Ripply3 function in the ectoderm and/or endoderm. Also, by monitoring AP-2α (Tcfap2α – Mouse Genome Informatics) and *Hand2* expression (Fig. 6K-N) (Chazaud et al., 1996; Srivastava et al., 1995), we confirmed that the neural crest cells failed to populate the third and fourth pharyngeal arches. The abnormal development of the neural crest cells might have resulted in the failure of cardiac development in the *Ripply3*$^{-/-}$ embryos.

Next, we examined the *Ripply3*$^{-/-}$ embryos for expression of several marker genes that are specifically expressed around the pharyngeal region. Expression of *Pax1* and *Pax9*, which is normally observed in the pharyngeal pouch endoderm (Wallin et al., 1996; Peters et al., 1998), was continuous rather than segmental in the endoderm posterior to the second pouch (Fig. 6O-R). Thus, most of the endoderm cells in the third and fourth arch regions had characteristics of the pharyngeal pouch in *Ripply3*$^{-/-}$ embryos. By contrast, *Gbx2* expression, a Tbx1 target in the pharyngeal ectoderm, was not changed in *Ripply3*$^{-/-}$ embryos (see Fig. S5 in the supplementary material) (Calmont et al., 2009), suggesting that *Ripply3*$^{-/-}$ embryos show no obvious defect in the pharyngeal ectoderm.

Enhancement of *Pax9* expression was specifically observed in the third and fourth arch regions in *Ripply3*-deficient embryos at ~E9.25-10.0 (Fig. 6Q,R; see Fig. S6 in the supplementary material). Thus, consistent with the in vitro luciferase assay indicating that Ripply3 can repress Tbx1-mediated *Pax9* expression (Fig. 2F,G), Ripply3 is likely to be involved in the repression of transcriptional activation by Tbx1 in vivo. In contrast to *Pax9*, the expression levels of *Pax1* and *Tbx1*, as well as those of Fgf-related genes including *Fgf8*, *Fgf3*, *Etv4* and *Etv5*, were not significantly changed in the third and fourth arch regions of *Ripply3*-deficient embryos (Fig. 6S-V; see Figs S7 and S8 in the supplementary material), although the expression domains of some of these genes were altered, probably owing to morphological changes in this region.

Comparison of the pharyngeal phenotype of *Ripply3* mutants with those of *Tbx1* mutants and *Tbx1;Ripply3* double mutants

Similar to *Ripply3*$^{-/-}$ embryos, *Tbx1*$^{-/-}$ embryos also lacked the characteristic segmental pattern of the caudal pharyngeal arches. However, we noted that the morphology of this region differed

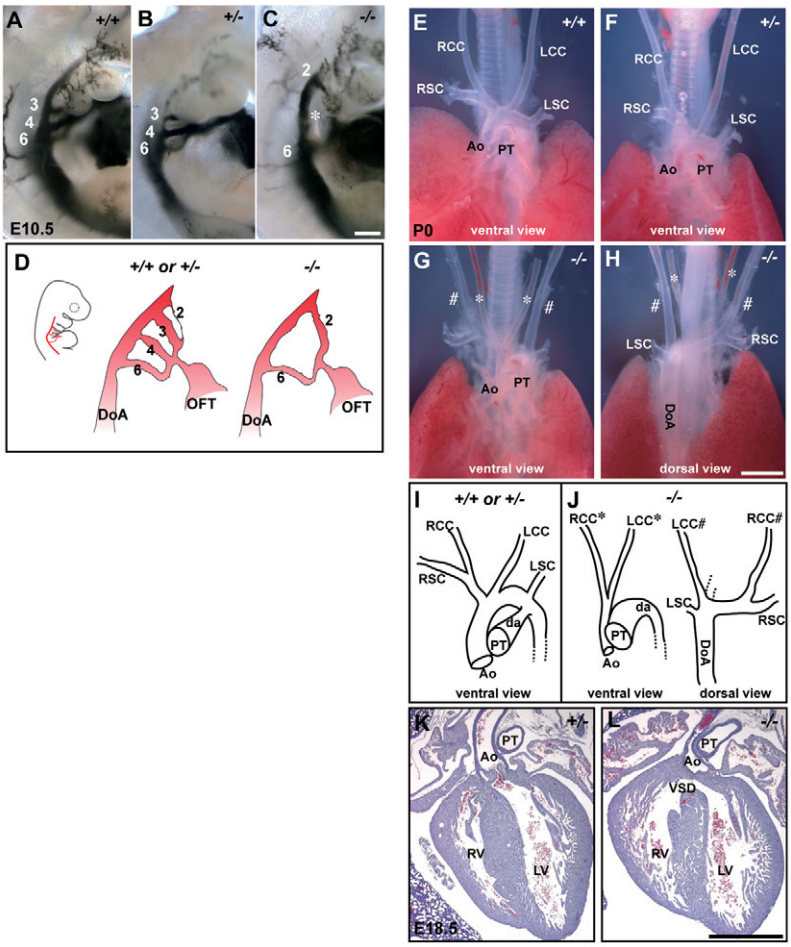

Fig. 4. Cardiovascular defects in *Ripply3*-deficient mice. (**A-C**) Typical morphology of pharyngeal arch arteries (PAAs) in wild-type (A), *Ripply3* heterozygous (B) and homozygous (C) mutant mice at E10.5 as visualized by intracardiac ink injection. The asterisk indicates the absence of the third and fourth PAAs in the *Ripply3*$^{-/-}$ embryo. (**D**) Schematic representation of the PAA pattern in A-C. (**E-H**) Anatomical analysis of great arteries in *Ripply3*$^{+/+}$ (E), *Ripply3*$^{+/-}$ (F), and *Ripply3*$^{-/-}$ (G,H) embryos at P0. Both left and right common carotid arteries are irregularly remodeled from persistent second PAAs (*) and dorsal aorta (#) in the *Ripply3*$^{-/-}$ embryo. Both right and left subclavian arteries are abnormally located on the dorsal side in the *Ripply3*$^{-/-}$ mutant (H). These abnormalities were observed in all *Ripply3*$^{-/-}$ mutants at P0 (n=26). (**I**,**J**) Schematic representation of the typical pattern of the outflow and great arteries in *Ripply3*$^{+/+}$, *Ripply3*$^{+/-}$ (I) and *Ripply3*$^{-/-}$ (J) embryos. (**K**,**L**) Hematoxylin and Eosin-stained hearts of *Ripply3*$^{+/-}$ (K) and *Ripply3*$^{-/-}$ (L) embryos at E18.5. A ventricular septal defect (VSD) is observed in *Ripply3*$^{-/-}$ embryos. Ao, aorta; DA, dorsal aorta; LCC, left common carotid; LSA, left subclavian artery; LV, left ventricle; RCC, right common carotid; RSA, right subclavian artery; PT, pulmonary trunk; RV, right ventricle. Scale bars: 200 μm in C; 1 mm in H,L.

between these two mutant embryos. As shown above, in the third and fourth arch regions of *Ripply3*$^{-/-}$ embryos, the entire ectoderm and endoderm layers were adjacent to each other, like those at the pharyngeal pouch, and endodermal pouch markers were expressed in almost all endoderm cells (Fig. 6B,D). By contrast, in *Tbx1*$^{-/-}$ embryos the ectoderm and endoderm layers were completely separated, and no characteristics of the pharyngeal pouch with respect to morphology or expression of molecular markers, including *Pax1*, were observed in the caudal pharyngeal region of these embryos (Fig. 7E; see Fig. S9 in the supplementary material) (Vitelli et al., 2002; Jerome and Papaioannou, 2001). Given that Ripply3 functions oppositely to Tbx1, this difference in phenotype in the third and fourth arch regions might be explained by the difference in their functions. Furthermore, as predicted from the in vitro luciferase assay showing that the function of Ripply3 is dependent on Tbx1, *Tbx1*$^{-/-}$;*Ripply3*$^{-/-}$ embryos exhibited a phenotype identical to that of *Tbx1*$^{-/-}$ embryos, and not to that of *Ripply3*$^{-/-}$ embryos, in the caudal pharyngeal region at E10.0-10.5 (Fig. 7E,F; see Fig. S9 in the supplementary material), as well as in the cardiovascular system at E17.5 (see Fig. S10 in the supplementary material).

Because *Tbx1* heterozygous mice frequently exhibit hypoplasia of their fourth PAAs, and a reduction in the activity of certain genes enhances this phenotype (Lindsay et al., 2001; Calmont et al., 2009), we also examined this phenotype in *Tbx1*$^{+/-}$;*Ripply3*$^{+/+}$ versus *Tbx1*$^{+/-}$;*Ripply3*$^{+/-}$ embryos. However, the penetrance and severity of this phenotype were not significantly changed by the dosage reduction to one copy of the *Ripply3* allele (Fig. 7B,C; see Table S2 in the supplementary material), suggesting that any interaction between Ripply3 and Tbx1 is not involved in the fourth PAA hypoplasia phenotype.

DISCUSSION

The role of Ripply3 in the development of the cardiovascular system

A striking feature of *Ripply3*$^{-/-}$ embryos is their almost complete lack of the third and fourth pharyngeal arches. In the area of these arches only a few mesodermal and neural crest cells were observed in the *Ripply3*$^{-/-}$ embryos. As *Ripply3* expression was not found in the mesoderm, nor in neural crest cells in the arches, the abnormal formation of the pharyngeal arches might be a consequence of the abnormal development of the pharyngeal endoderm, in which *Ripply3* is expressed.

The disrupted development of the caudal pharyngeal arches appears to have resulted in two distinct cardiovascular defects in *Ripply3*$^{-/-}$ embryos. One involved an abnormality in heart development. The reduction in neural crest cell number in the caudal pharyngeal arches appears to have led to the abnormal development of the outflow tract, including hypotrophy of the aorta and incomplete formation of the ventricular septum. However, in spite of the reduction in the number of neural crest cells in the third and fourth arches, the formation of the outflow septum, which is

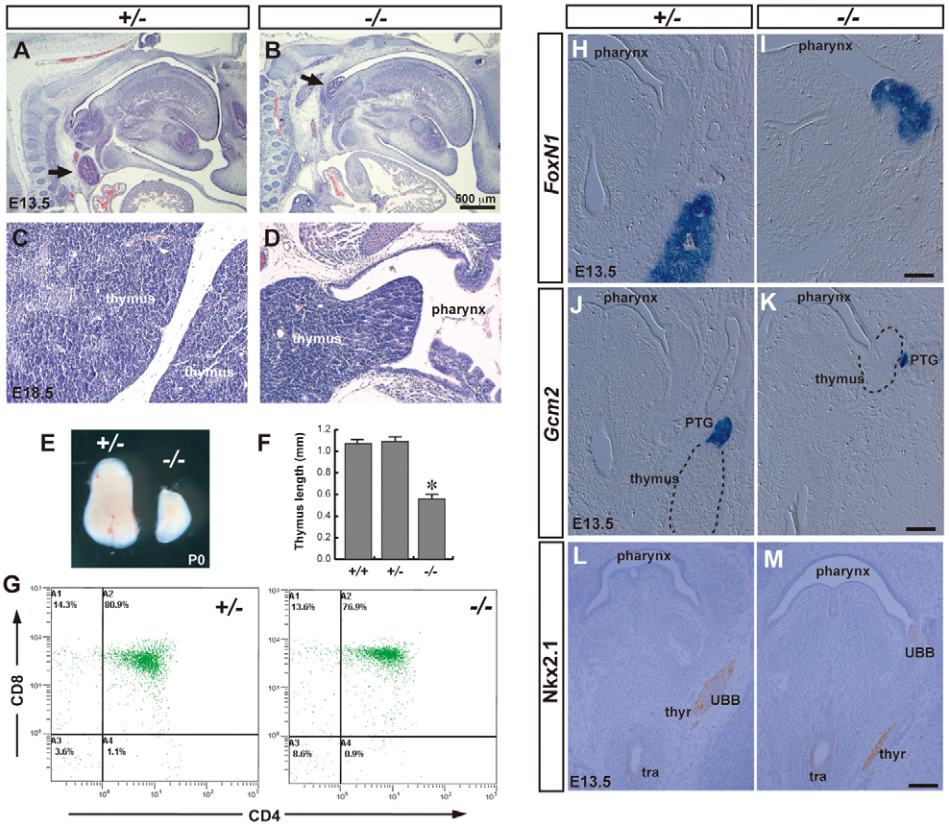

Fig. 5. Defects in the development of pharyngeal pouch-derived organs in *Ripply3*-deficient embryos. (**A-D**) Migration phenotype in the thymic lobes. Sagittal sections of *Ripply3*$^{+/-}$ (A) and *Ripply3*$^{-/-}$ (B) embryos at E13.5 stained with Hematoxylin and Eosin are shown. The thymic lobe is ectopically located in the oropharynx of the *Ripply3*$^{-/-}$ embryo (B). Arrows indicate the thymus. Sections of thymus from a *Ripply3*$^{+/-}$ (C) and *Ripply3*$^{-/-}$ (D) embryo at E18.5 are shown. (**E**) Size reduction of the *Ripply3*$^{-/-}$ thymus at P0. (**F**) Comparison of thymus size in terms of length. *, $P<0.001$. Error bars indicate mean + s.e.m. (**G**) Flow cytometry comparing CD4 and CD8 expression in thymocytes prepared from the thymus of newborn *Ripply3*$^{+/-}$ and *Ripply3*$^{-/-}$ mice. (**H-M**) Migration defects in the thymus, parathyroid gland (PTG) and ultimobranchial body (UBB) in *Ripply3*$^{-/-}$ mutants. (H-K) In situ hybridization for *Foxn1*, a marker of the thymic epithelium (H,I), and for *Gcm2*, a marker of the parathyroid gland (J,K), in *Ripply3*$^{+/-}$ (H,J) and *Ripply3*$^{-/-}$ (I,K) embryos. (L,M) Immunostaining with anti-Nkx2.1 antibody, which is specific for the thyroid and ultimobranchial body, in *Ripply3*$^{+/-}$ (L) and *Ripply3*$^{-/-}$ (M) embryos. The ultimobranchial body contains cells weakly positive for Nkx2.1. thyr, thyroid gland; tra, trachea. Scale bars: 500 μm in A,B; 50 μm in H-M.

also orchestrated by neural crest cells, was achieved in *Ripply3*$^{-/-}$ embryos. Thus, we speculate that the reduction in the number of neural crest cells might not have been so severe as to cause a separation defect in the outflow tract or that neural crest cells migrating through the sixth pharyngeal arches might have contributed to septum formation. The other defect involved the loss of the third and fourth PAAs. This defect appeared to result in abnormal development of the vascular system, including deletion of the aortic arch and misshapen major blood vessels.

Interestingly, the second PAAs, which normally disappear after E10.5, persisted until birth in *Ripply3*$^{-/-}$ embryos. Persistence of the first and second PAAs has also been reported in endothelin 1-deficient mouse embryos, in which the fourth PAAs are also poorly developed, suggesting that the formation of PAAs proximal to the heart might be a prerequisite for the regression of the more distal PAAs (Kurihara et al., 1995). We speculate that development of the proximal PAAs resulted in a decrease in blood flow running through the existing distal PAAs, which in turn decreased the mechanical stress caused by blood flow, making it virtually impossible for the distal PAAs to be maintained (Yashiro et al., 2007).

The role of Ripply3 in pharyngeal endoderm development

Ripply3 expression in the developing pharyngeal apparatus was dynamic and was observed in endoderm and ectoderm cells in the pouches and in the caudal pharyngeal region, suggesting that Ripply3 plays specific roles in these cells. In the *Ripply3*$^{-/-}$ embryos, phenotypic abnormalities were first identified in the pharyngeal pouches forming posterior to the second arch. In these embryos, *Pax1* and *Pax9*, which are specifically expressed in the pharyngeal pouches of normal embryos (Wallin et al., 1996; Peters et al., 1998), are uniformly expressed throughout the entire pharyngeal endoderm region posterior to the second pouch. Thus, it appears that Ripply3 activity is required for the proper development of the posterior pharyngeal arches, although it remains unclear why only caudal pouches were affected in the *Ripply3*$^{-/-}$ embryos.

In the later stages of mouse development the caudal pharyngeal pouches give rise to several organs, including the thymus, parathyroid glands and ultimobranchial bodies (Manley and Capecchi, 1998; Kusakabe et al., 2006). The primordia of these organs become specified at particular positions around the pouches,

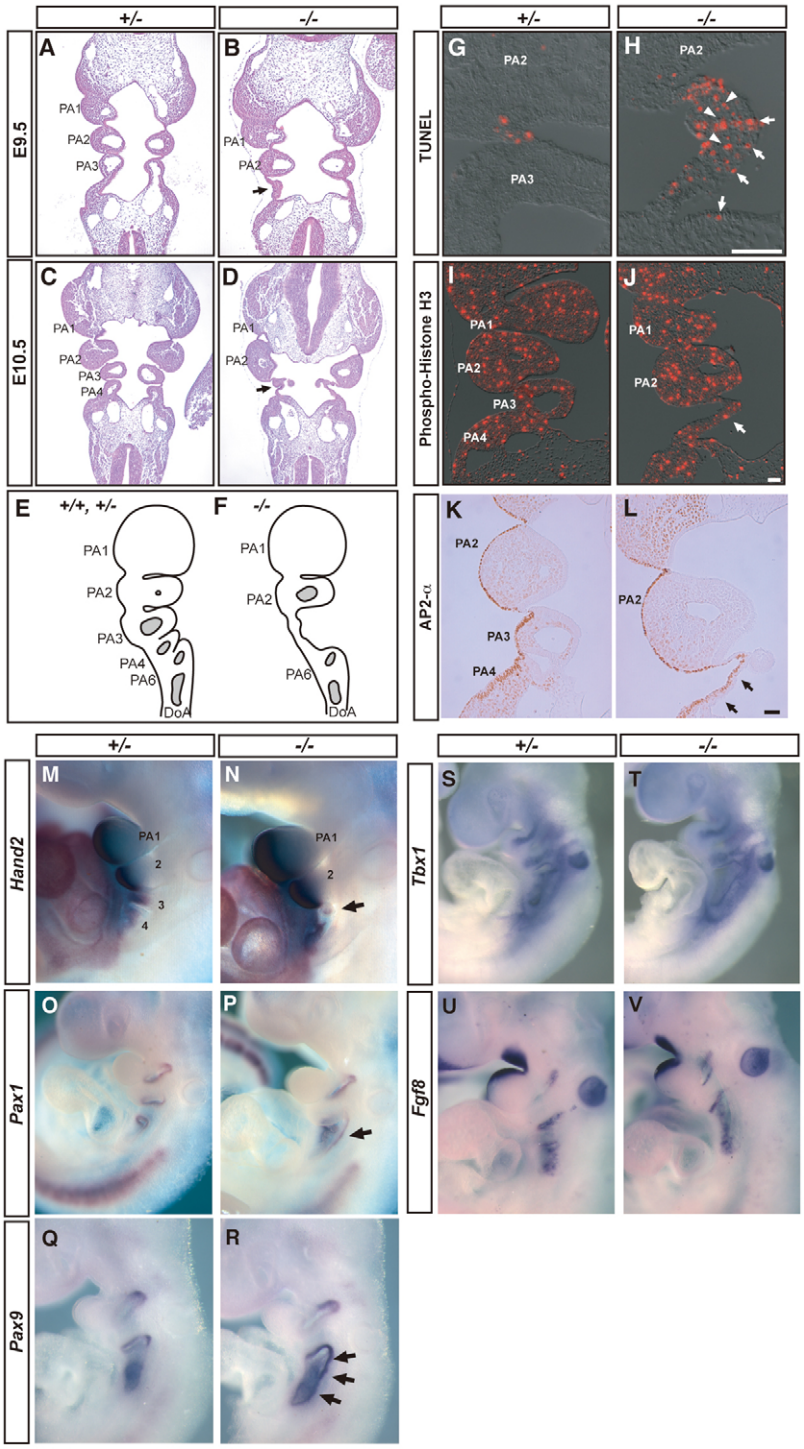

Fig. 6. *Ripply3* is required for proper development of the third and fourth pharyngeal arches. (**A-D**) Hematoxylin and Eosin-stained coronal sections of *Ripply3*$^{+/-}$ (A,C) and *Ripply3*$^{-/-}$ (B,D) embryos at E9.5 (A,B) and E10.5 (C,D). (**E**,**F**) Schematic illustrations of the phenotypes of *Ripply3*$^{+/-}$ (E) and *Ripply3*$^{-/-}$ (F) embryos. (**G**,**H**) Apoptotic cells detected by TUNEL in *Ripply3*$^{+/-}$ (G) and *Ripply3*$^{-/-}$ (H) embryos at E10.5. Arrows indicate apoptotic cells in the endoderm cell population and arrowheads indicate those in the mesoderm and/or neural crest cell population. (**I**,**J**) Mitotic cells labeled with anti-phospho-histone H3 antibody in *Ripply3*$^{+/-}$ (I) and *Ripply3*$^{-/-}$ (J) embryos at E10.5. (**K**,**L**) Neural crest cells stained with anti-AP-2α antibody in the pharyngeal arch (PA) of *Ripply3*$^{+/-}$ (K) and *Ripply3*$^{-/-}$ (L) embryos at E10.5. (**M-V**) Whole-mount in situ hybridization with pharyngeal arch markers on *Ripply3*$^{+/-}$ (M,O,Q,S,U) and *Ripply3*$^{-/-}$ (N,P,R,T,V) embryos at E9.5-10.5 with probes for *Hand2* (M,N), *Pax1* (O,P), *Pax9* (Q,R), *Tbx1* (S,T) and *Fgf8* (U,V). Arrows (B,D,J,L,N,P,R) indicate abnormal third and fourth PA regions in *Ripply3*$^{-/-}$ mutants. Scale bars: 50 μm.

separate from the epithelial sheet of the pharyngeal pouch, and migrate ventrocaudally before reaching their final adult positions. The precise molecular mechanisms underling these processes remain to be elucidated. In *Ripply3*$^{-/-}$ embryos, the thymus, parathyroid glands and ultimobranchial bodies did not separate from the pharyngeal endoderm but maturated ectopically. This suggests that Ripply3 is specifically required for the separation processes that result in the development of these organs from the pharyngeal epithelial sheets. By contrast, specification and differentiation of these primordia were not affected by the absence of Ripply3 activity, although some of these organs appeared smaller than those in normal embryos. Thus, Ripply3 is unlikely to be required for the specification and maturation of the organ primordium. These results suggest that the mechanisms underlying the movement of the organ primordium differ from those that are required for their specification and maturation.

The development of the thymus and parathyroid glands is also abnormal in mouse embryos exhibiting altered *Tbx1* dosages (Liao et al., 2004; Zhang and Baldini, 2008). Whereas *Tbx1* null mutants exhibit a complete lack of thymus and parathyroid glands, embryos

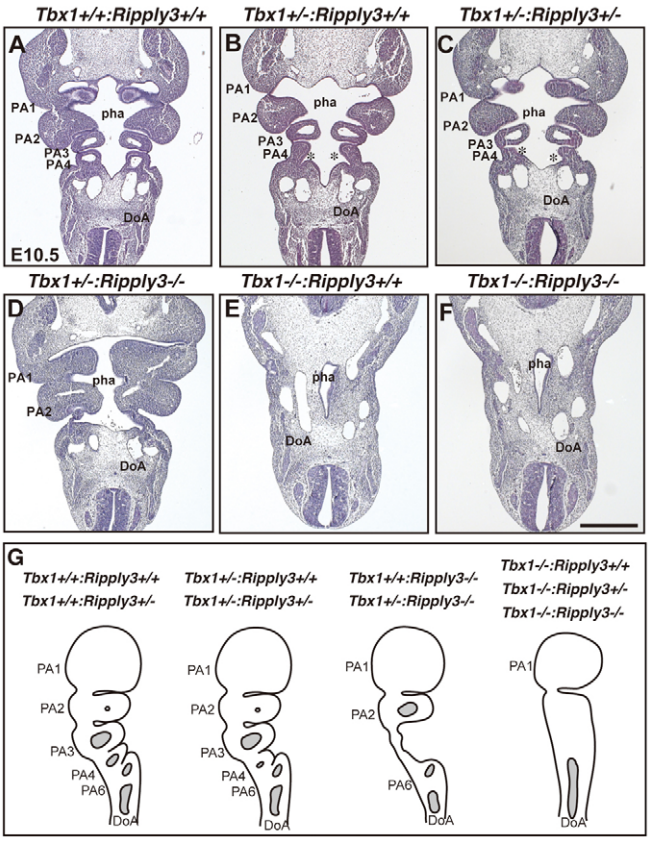

Fig. 7. Pharyngeal arch phenotype in *Tbx1;Ripply3* double-knockout mutants. (**A-F**) Hematoxylin and Eosin staining of coronal sections of *Tbx1*$^{+/+}$;*Ripply3*$^{+/+}$ (A), *Tbx1*$^{+/+}$;*Ripply3*$^{+/-}$ (B), *Tbx1*$^{+/-}$;*Ripply3*$^{+/-}$ (C), *Tbx1*$^{+/-}$;*Ripply3*$^{-/-}$ (D), *Tbx1*$^{-/-}$;*Ripply3*$^{+/+}$ (E) and *Tbx1*$^{-/-}$;*Ripply3*$^{-/-}$ (F) embryos at E10.5. (**G**) Schematic representation of the pharyngeal phenotypes of each genotype. PA, pharyngeal arch; pha, pharynx; DoA, dorsal aorta. Asterisks indicate the hypotrophic fourth PAAs. Scale bar: 500 μm.

with an increased *Tbx1* dosage frequently exhibit ectopic thymus and parathyroid glands. Thus, Tbx1 appears to play an important role in several distinct aspects of the development of these organs, including their growth and migration. Given that the development of these organs in *Ripply3*-deficient embryos partly resembles that of mouse embryos overexpressing Tbx1 (Merscher et al., 2001; Liao et al., 2004), we presume that Ripply3-mediated repression of Tbx1 activity was involved in the Tbx1-mediated migration of these primordia from the pharyngeal endoderm.

Interestingly, ectopic location of the thymus has also been reported in several mouse mutants, as well as in humans. For instance, *Pax9*-deficient mouse embryos exhibit an ectopic thymus located in the larynx, as in the case of *Ripply3*-deficient mice, suggesting that there is interplay between Pax9 and Ripply3 in the movement of the thymus primordium (Hetzer-Egger et al., 2002). However, in contrast to Pax9-deficient embryos, we showed that expression of *Pax9* was not reduced, but rather increased, in the pharyngeal endoderm in *Ripply3*-deficient embryos. Thus, too much or too little Pax9 appears to inhibit proper migration of the thymus primordium. One of the roles of Ripply3 might be the maintenance of an adequate expression level of *Pax9* in the pharyngeal endoderm.

Modulation of Tbx1 activity by Ripply3

In addition to the resemblance in pharyngeal phenotype, many other results of this study support the idea that Ripply3 represses the function of Tbx1 in the pharyngeal endoderm. We showed by in situ hybridization that *Ripply3* and *Tbx1* are strongly co-expressed in the caudal pharyngeal endoderm. We also showed that the transcriptional activity of mouse Tbx1 is repressed by mouse Ripply3. In addition, the expression of *Pax9*, a downstream gene activated by Tbx1, was upregulated in Ripply3-deficient embryos. Thus, we speculate that Ripply3-mediated repression of Tbx1 activity is crucial for the normal development of the pharyngeal derivatives.

During pharyngeal development, Tbx1 is expressed in multiple cell types, including endodermal, mesodermal and ectodermal cells (Chapman et al., 1996; Vitelli et al., 2002; Yamagishi et al., 2003). Conditional gene knockout in the endoderm or mesoderm indicates that Tbx1 has specific roles in these tissues (Arnold et al., 2006; Zhang et al., 2006). In addition, *Tbx1* is required for gene expression in the pharyngeal ectoderm (Calmont et al., 2009). Thus, Tbx1 plays multiple roles in endodermal, mesodermal and ectodermal cells during pharyngeal development. Because it is not expressed in the mesoderm, Ripply3 would appear to modulate the function of Tbx1 in a cell type-specific manner. In this study, we also showed that hypoplasia of the fourth PAAs, which is frequently observed in *Tbx1* heterozygous mice, was not significantly changed by dosage reduction to one copy of the *Ripply3* allele. Since *Ripply3* is specifically expressed in the pharyngeal endoderm and ectoderm, but not in the mesoderm, this dosage reduction of Ripply3 was unlikely to affect the activity of Tbx1 in the mesoderm, which appears to be important for the development of PAAs. Thus, our finding of no significant enhancement of the PAA hypoplasia phenotype by dosage reduction of *Ripply3* might represent cell type-specific regulation of Tbx1 by Ripply3.

In the pharyngeal endoderm, expression of *Pax9*, a target of Tbx1, was upregulated in *Ripply3*-deficient embryos. Thus, Ripply3 appears to control Tbx1 activity in the pharyngeal endoderm. Interestingly, alterations in the gene dosage of *Tbx1*, in addition to those in its mRNA level, have been shown to result in a wide range of phenotypes, suggesting that Tbx1 activity is tightly controlled during pharyngeal development (Liao et al., 2004; Zhang and Baldini, 2008). Given that *Pax9* is expressed at some particular level in wild-type embryos even in the presence of Ripply3, we propose that Ripply3-mediated repression contributes to the stringent control of Tbx1 activity in the pharyngeal endoderm.

In summary, we have identified a key gene that acts cooperatively with Tbx1 in the development of the pharyngeal apparatus and its derivatives. Our results suggest that Tbx1 activity is modulated in the pharyngeal endoderm in a Ripply3 expression-dependent manner. Our findings provide new insight into the molecular mechanisms underlying the development of the pharyngeal apparatus.

Acknowledgements

We thank Dr N. Takeda of Kumamoto University for the blastocyst injection; Drs S. Kobayashi, C. Noda, M. Sasaki, A. Ohbayashi, N. Ohbayashi, S. Arai, R. Takada, Mr T. Yokota and Ms M. Furutani for technical support; Drs B. Morrow, B. Hogan, N. Manley, P. Gruss and A. Baldini for providing materials; and Dr A. Sato and members of the S.T. lab for helpful discussions. This work was supported in part by a grant-in-aid for scientific research (S.T. and T.O.) and by the Program for Promoting the Establishment of Strategic Research Centers, Special Coordination Funds for Promoting Science and Technology (R.M.) from the Ministry of Education, Culture, Sports, Science and Technology of Japan.

Competing interests statement

The authors declare no competing financial interests.

Supplementary material

Supplementary material for this article is available at
http://dev.biologists.org/lookup/suppl/doi:10.1242/dev.054056/-/DC1

References

Arnold, J. S., Braunstein, E. M., Ohyama, T., Groves, A. K., Adams, J. C., Brown, M. C. and Morrow, B. E. (2006). Tissue-specific roles of Tbx1 in the development of the outer, middle and inner ear, defective in 22q11DS patients. *Hum. Mol. Genet.* **15**, 1629-1639.

Baldwin, H. S., Shen, H. M., Yan, H. C., DeLisser, H. M., Chung, A., Mickanin, C., Trask, T., Kirschbaum, N. E., Newman, P. J., Albelda, S. M. et al. (1994). Platelet endothelial cell adhesion molecule-1 (PECAM-1/CD31): alternatively spliced, functionally distinct isoforms expressed during mammalian cardiovascular development. *Development* **120**, 2539-2553.

Calmont, A., Ivins, S., Van Bueren, K. L., Papangeli, I., Kyriakopoulou, V., Andrews, W. D., Martin, J. F., Moon, A. M., Illingworth, E. A., Basson, M. A. et al. (2009). Tbx1 controls cardiac neural crest cell migration during arch artery development by regulating Gbx2 expression in the pharyngeal ectoderm. *Development* **136**, 3173-3183.

Chan, T., Kondow, A., Hosoya, A., Hitachi, K., Yukita, A., Okabayashi, K., Nakamura, H., Ozawa, H., Kiyonari, H., Michiue, T. et al. (2007). Ripply2 is essential for precise somite formation during mouse early development. *FEBS Lett.* **581**, 2691-2696.

Chapman, D. L., Garvey, N., Hancock, S., Alexiou, M., Agulnik, S. I., Gibson-Brown, J. J., Cebra-Thomas, J., Bollag, R. J., Silver, L. M. and Papaioannou, V. E. (1996). Expression of the T-box family genes, Tbx1-Tbx5, during early mouse development. *Dev. Dyn.* **206**, 379-390.

Chazaud, C., Oulad-Abdelghani, M., Bouillet, P., Decimo, D., Chambon, P. and Dolle, P. (1996). AP-2.2, a novel gene related to AP-2, is expressed in the forebrain, limbs and face during mouse embryogenesis. *Mech. Dev.* **54**, 83-94.

Fulcoli, F. G., Huynh, T., Scambler, P. J. and Baldini, A. (2009). Tbx1 regulates the BMP-Smad1 pathway in a transcription independent manner. *PLoS ONE* **4**, e6049.

Gordon, J., Bennett, A. R., Blackburn, C. C. and Manley, N. R. (2001). Gcm2 and Foxn1 mark early parathyroid- and thymus-specific domains in the developing third pharyngeal pouch. *Mech. Dev.* **103**, 141-143.

Hetzer-Egger, C., Schorpp, M., Haas-Assenbaum, A., Balling, R., Peters, H. and Boehm, T. (2002). Thymopoiesis requires Pax9 function in thymic epithelial cells. *Eur. J. Immunol.* **32**, 1175-1181.

Hitachi, K., Danno, H., Tazumi, S., Aihara, Y., Uchiyama, H., Okabayashi, K., Kondow, A. and Asashima, M. (2009). The Xenopus Bowline/Ripply family proteins negatively regulate the transcriptional activity of T-box transcription factors. *Int. J. Dev. Biol.* **53**, 631-639.

Hu, T., Yamagishi, H., Maeda, J., McAnally, J., Yamagishi, C. and Srivastava, D. (2004). Tbx1 regulates fibroblast growth factors in the anterior heart field through a reinforcing autoregulatory loop involving forkhead transcription factors. *Development* **131**, 5491-5502.

Ivins, S., Lammerts van Beuren, K., Roberts, C., James, C., Lindsay, E., Baldini, A., Ataliotis, P. and Scambler, P. J. (2005). Microarray analysis detects differentially expressed genes in the pharyngeal region of mice lacking Tbx1. *Dev. Biol.* **285**, 554-569.

Jerome, L. A. and Papaioannou, V. E. (2001). DiGeorge syndrome phenotype in mice mutant for the T-box gene, Tbx1. *Nat. Genet.* **27**, 286-291.

Kawamura, A., Koshida, S., Hijikata, H., Ohbayashi, A., Kondoh, H. and Takada, S. (2005). Groucho-associated transcriptional repressor ripply1 is required for proper transition from the presomitic mesoderm to somites. *Dev. Cell* **9**, 735-744.

Kawamura, A., Koshida, S. and Takada, S. (2008). Activator-to-repressor conversion of T-box transcription factors by the Ripply family of Groucho/TLE-associated mediators. *Mol. Cell. Biol.* **28**, 3236-3244.

Kondow, A., Hitachi, K., Ikegame, T. and Asashima, M. (2006). Bowline, a novel protein localized to the presomitic mesoderm, interacts with Groucho/TLE in Xenopus. *Int. J. Dev. Biol.* **50**, 473-479.

Kondow, A., Hitachi, K., Okabayashi, K., Hayashi, N. and Asashima, M. (2007). Bowline mediates association of the transcriptional corepressor XGrg-4 with Tbx6 during somitogenesis in Xenopus. *Biochem. Biophys. Res. Commun.* **359**, 959-964.

Kurihara, Y., Kurihara, H., Oda, H., Maemura, K., Nagai, R., Ishikawa, T. and Yazaki, Y. (1995). Aortic arch malformations and ventricular septal defect in mice deficient in endothelin-1. *J. Clin. Invest.* **96**, 293-300.

Kusakabe, T., Hoshi, N. and Kimura, S. (2006). Origin of the ultimobranchial body cyst: T/ebp/Nkx2.1 expression is required for development and fusion of the ultimobranchial body to the thyroid. *Dev. Dyn.* **235**, 1300-1309.

Liao, J., Kochilas, L., Nowotschin, S., Arnold, J. S., Aggarwal, V. S., Epstein, J. A., Brown, M. C., Adams, J. and Morrow, B. E. (2004). Full spectrum of malformations in velo-cardio-facial syndrome/DiGeorge syndrome mouse models by altering Tbx1 dosage. *Hum. Mol. Genet.* **13**, 1577-1585.

Liao, J., Aggarwal, V. S., Nowotschin, S., Bondarev, A., Lipner, S. and Morrow, B. E. (2008). Identification of downstream genetic pathways of Tbx1 in the second heart field. *Dev. Biol.* **316**, 524-537.

Lindsay, E. A., Vitelli, F., Su, H., Morishima, M., Huynh, T., Pramparo, T., Jurecic, V., Ogunrinu, G., Sutherland, H. F., Scambler, P. J. et al. (2001). Tbx1 haploinsufficiency in the DiGeorge syndrome region causes aortic arch defects in mice. *Nature* **410**, 97-101.

Manley, N. R. and Capecchi, M. R. (1998). Hox group 3 paralogs regulate the development and migration of the thymus, thyroid, and parathyroid glands. *Dev. Biol.* **195**, 1-15.

Merscher, S., Funke, B., Epstein, J. A., Heyer, J., Puech, A., Lu, M. M., Xavier, R. J., Demay, M. B., Russell, R. G., Factor, S. et al. (2001). TBX1 is responsible for cardiovascular defects in velo-cardio-facial/DiGeorge syndrome. *Cell* **104**, 619-629.

Moreno, T. A., Jappelli, R., Belmonte, J. C. and Kintner, C. (2008). Retinoic acid regulation of the Mesp-Ripply feedback loop during vertebrate segmental patterning. *Dev. Biol.* **315**, 317-330.

Morimoto, M., Sasaki, N., Oginuma, M., Kiso, M., Igarashi, K., Aizaki, K., Kanno, J. and Saga, Y. (2007). The negative regulation of Mesp2 by mouse Ripply2 is required to establish the rostro-caudal patterning within a somite. *Development* **134**, 1561-1569.

Ohbayashi, N., Shibayama, M., Kurotaki, Y., Imanishi, M., Fujimori, T., Itoh, N. and Takada, S. (2002). FGF18 is required for normal cell proliferation and differentiation during osteogenesis and chondrogenesis. *Genes Dev.* **16**, 870-879.

Paylor, R., Glaser, B., Mupo, A., Ataliotis, P., Spencer, C., Sobotka, A., Sparks, C., Choi, C. H., Oghalai, J., Curran, S. et al. (2006). Tbx1 haploinsufficiency is linked to behavioral disorders in mice and humans: implications for 22q11 deletion syndrome. *Proc. Natl. Acad. Sci. USA* **103**, 7729-7734.

Peters, H., Neubuser, A., Kratochwil, K. and Balling, R. (1998). Pax9-deficient mice lack pharyngeal pouch derivatives and teeth and exhibit craniofacial and limb abnormalities. *Genes Dev.* **12**, 2735-2747.

Scambler, P. J. (2000). The 22q11 deletion syndromes. *Hum. Mol. Genet.* **9**, 2421-2426.

Shibuya, K., Kudoh, J., Minoshima, S., Kawasaki, K., Asakawa, S. and Shimizu, N. (2000). Isolation of two novel genes, DSCR5 and DSCR6, from Down syndrome critical region on human chromosome 21q22.2. *Biochem. Biophys. Res. Commun.* **271**, 693-698.

Srivastava, D. and Olson, E. N. (2000). A genetic blueprint for cardiac development. *Nature* **407**, 221-226.

Srivastava, D., Cserjesi, P. and Olson, E. N. (1995). A subclass of bHLH proteins required for cardiac morphogenesis. *Science* **270**, 1995-1999.

Stoller, J. Z. and Epstein, J. A. (2005). Identification of a novel nuclear localization signal in Tbx1 that is deleted in DiGeorge syndrome patients harboring the 1223delC mutation. *Hum. Mol. Genet.* **14**, 885-892.

Takahashi, J., Ohbayashi, A., Oginuma, M., Saito, D., Mochizuki, A., Saga, Y. and Takada, S. (2010). Analysis of Ripply1/2-deficient mouse embryos reveals a mechanism underlying the rostro-caudal patterning within a somite. *Dev. Biol.* **342**, 134-145.

Vitelli, F., Morishima, M., Taddei, I., Lindsay, E. A. and Baldini, A. (2002). Tbx1 mutation causes multiple cardiovascular defects and disrupts neural crest and cranial nerve migratory pathways. *Hum. Mol. Genet.* **11**, 915-922.

Wallin, J., Eibel, H., Neubuser, A., Wilting, J., Koseki, H. and Balling, R. (1996). Pax1 is expressed during development of the thymus epithelium and is required for normal T-cell maturation. *Development* **122**, 23-30.

Xu, H., Morishima, M., Wylie, J. N., Schwartz, R. J., Bruneau, B. G., Lindsay, E. A. and Baldini, A. (2004). Tbx1 has a dual role in the morphogenesis of the cardiac outflow tract. *Development* **131**, 3217-3227.

Yagi, H., Furutani, Y., Hamada, H., Sasaki, T., Asakawa, S., Minoshima, S., Ichida, F., Joo, K., Kimura, M., Imamura, S. et al. (2003). Role of TBX1 in human del22q11.2 syndrome. *Lancet* **362**, 1366-1373.

Yamagishi, H., Maeda, J., Hu, T., McAnally, J., Conway, S. J., Kume, T., Meyers, E. N., Yamagishi, C. and Srivastava, D. (2003). Tbx1 is regulated by tissue-specific forkhead proteins through a common Sonic hedgehog-responsive enhancer. *Genes Dev.* **17**, 269-281.

Yashiro, K., Shiratori, H. and Hamada, H. (2007). Haemodynamics determined by a genetic programme govern asymmetric development of the aortic arch. *Nature* **450**, 285-288.

Yoshikawa, Y., Fujimori, T., McMahon, A. P. and Takada, S. (1997). Evidence that absence of Wnt-3a signaling promotes neuralization instead of paraxial mesoderm development in the mouse. *Dev. Biol.* **183**, 234-242.

Zhang, Z. and Baldini, A. (2008). In vivo response to high-resolution variation of Tbx1 mRNA dosage. *Hum. Mol. Genet.* **17**, 150-157.

Zhang, Z., Huynh, T. and Baldini, A. (2006). Mesodermal expression of Tbx1 is necessary and sufficient for pharyngeal arch and cardiac outflow tract development. *Development* **133**, 3587-3595.

Zweier, C., Sticht, H., Aydin-Yaylagul, I., Campbell, C. E. and Rauch, A. (2007). Human TBX1 missense mutations cause gain of function resulting in the same phenotype as 22q11.2 deletions. *Am. J. Hum. Genet.* **80**, 510-517.

Table S1. Ratio of *Ripply3* mutant embryos and pups

		Genotype		
Stage	Number	+/+	+/–	–/–
E16.5	25	6	11	8
E17.5	32	10	22	10
E18.5	100	25	53	22
Newborn	115	25	64	26*
Total	282	66	150	66
Percentage		23.4	53.2	23.4

*Eight pups out of 26 were dead; the others survived but had cyanosis.

Table S2. Defect of the fourth pharyngeal arch artery in compound heterozygotes at E10.0-11.5

Genotype	Normal	Unilateral	Bilateral	Total
Tbx1$^{+/-}$;*Ripply3*$^{+/+}$	2	3	7	12
	16.7%	25.0%	58.3%	
Tbx1$^{+/-}$;*Ripply3*$^{+/-}$	1	5	9	15
	6.7%	33.3%	60.0%	